Supplementary Materials

Supplementary Table S1. Structural statistics for the family of 20 structures of FUS-RRM in aqueous solution.

Distance restraints	
Intraresidue (i-j=0)	719
Sequential (|i-j|=1)	425
Medium range ($2 \leq \|i-j\| \leq 4$)	186
Long range ($\|i-j\| \geq 5$)	328
Hydrogen bonds	18
Total	1676
Dihedral angle restraints	
Φ	47
Ψ	47
Total	94
Mean r.m.s. deviations from the experimental restraints	
Distance (Å)	0.0185±0.0012
Dihedral angle (^{o})	0.2265±0.0479
Mean r.m.s. deviations from idealized covalent geometry	
Bond (Å)	0.0020±0.00012
Angle (^{o})	0.3653±0.0166
Improper (^{o})	0.2407±0.0206
Mean energies (kcal mol^{-1})[a]	
E_{NOE}	28.85±3.85
E_{cdih}	0.31±0.13
E_{L-J}	-189.01±24.74
Ramachandran plot[b]	
Residues 286-292, 295-327 and 336-368 in FUS-RRM	
% residues in the most favorable regions	80.4
additional allowed regions	17.5
generously allowed regions	1.5
Atomic r.m.s. differences (Å)	
Residues 286-292, 295-327 and 336-368 in FUS-RRM	
Backbone heavy atoms (N, Cα, and C')	0.454
Heavy atoms	0.922

None of the structures exhibits distance violations greater than 0.3 Å or dihedral angle violations greater than 4˚.

[a]The final values of the square-well NOE and dihedral angle potentials were calculated with force constants of 50 kcal mol^{-1}Å^{-1} and 200 kcal mol^{-1}rad^{-1}.

[b]The program PROCHECK (http://www.biochem.ucl.ac.uk/~roman/procheck_nmr/procheck_nmr.html) was used to assess the overall quality of the structures.

Figure S1. The FUS-RRM domain is distinct from other hnRNP RRM domains. (A) Ribbon diagram of a classical RRM structure showing the typical β1α1β2β3α2β4 RRM-fold. (B) Structure-based sequence alignment of the RRM domains generated by Dali Server (http://ekhidna.biocenter.helsinki.fi/dali_server). The secondary structures of the FUS-RRM domain are marked on the top. The RNP1 and RNP2 regions are highlighted with red boxes with the consensus sequences shown at the bottom. The extra long L2 loop is highlighted with a black box. Telomeric DNA binding sites of hnRNP A1 RRM1 are enclosed in small red box, and the corresponding residues of hnRNP D1 BD2 and FUS-RRM are enclosed in green box.

Figure S2. The ^{1}H-^{15}N HSQC spectrum of the FUS-RRM domain. The spectrum showed good peak dispersion and peak intensity. Each peak in the spectrum was labeled with residue number and the much crowded areas in the middle were enlarged.

Figure S3. Chemical shift perturbations in FUS-RRM upon titration with different nucleic acids. (A-D) Overlay plots of the ^{1}H-^{15}N HSQC spectra of the FUS-RRM domain and that of the domain titrated with RNA (UAGUUUGGUGAU) (A), 6-mer DNA (d(TTAGGG)) (B), 24-mer DNA (d(TTAGGG)$_4$) (C) and ds-DNA (d(TTAGGG/CCCTAA)$_4$) (D). The peaks with significant chemical shift changes are marked and the changes are highlighted by green arrows.

Figure S4. Comparison of the nucleic acid binding interfaces between FUS-RRM and BD2 of hnRNP D. The structures of FUS-RRM (A-B) and the BD2 domain of hnRNP D (C-D) are shown in the ribbon diagrams. The residues responsible for binding to nucleic acids were determined from NMR chemical shift perturbations and are highlighted in red. (**A**) FUS-RRM and 6-mer DNA d(TTAGGG)$_4$; (**B**) FUS-RRM and RNA UAGUUUGGUGAU; (**C**) BD2 of hnRNP D and 6-mer DNA d(TTAGGG); (**D**) BD2 of hnRNP D and RNA UUAGGG.

Figure S5. The conformations of the nucleic acids. (A) Overlay CD spectra of the 6-mer, 24-mer and ds-DNA. Each DNA sample gives a distinct CD characteristic of single-stranded, quadruplex and double-stranded DNA, respectively. (B) The CD spectra of 24-mer DNA upon addition of different amounts of protein. (C) The CD spectra of ds-DNA upon addition of different amounts of protein. (B) and (C) support that the conformation of nucleic acids remained largely unchanged upon addition of FUS-RRM.

Figure S6. Curve fitting of the chemical shift changes upon binding to nucleic acid at different concentrations. The dissociation constants of the FUS-RRM interaction with RNA (A, UAGUUUGGUGAU), 6-mer DNA (B, d(TTAGGG)) and dsDNA (C, d(TTAGGG/CCCTAA)$_4$) for selected residues are calculated by curve fitting the function describe in material and method section and the results are shown on the right. The selected residues are in different contacting clusters of the RRM

domain and their residue numbers are labeled in the black box of each panel.

Figure S7. The concentration response curve of FUS-RRM binding to various forms of nucleic acids. The nucleic acids used in the surface plasmon resonance (SPR) experiments were: RNA, UAGUUUGGUGAU; 6-mer DNA, d(TTAGGG); 24-mer DNA, $d(TTAGGG)_4$ and ds-DNA $d(TTAGGG/CCCTAA)_4$. The stoichiometry of FUS-RRM binding to nucleic acids was estimated in the SPR experiments. The FUS-RRM bound to RNA and 6-mer DNA with an approximate 1:1 ratio whereas the ratio of FUS-RRM to the G-quadruplex and ds-DNA was approximately 2:1 and 3.5:1, respectively.

Figure S8. Site-directed mutation has minimal effects on the overall structure of the FUS-RRM domain. An overlay plot of the ^{1}H-^{15}N HSQC spectra of the wild-type FUS-RRM domain (black), K312A/K315A/K316A (red). The NMR spectra were nearly identical with virtually no significant chemical shift changes expect for the "KK" loop region and close neighbors, demonstrating that the mutations do not change the global 3D structure of the FUS-RRM domain.

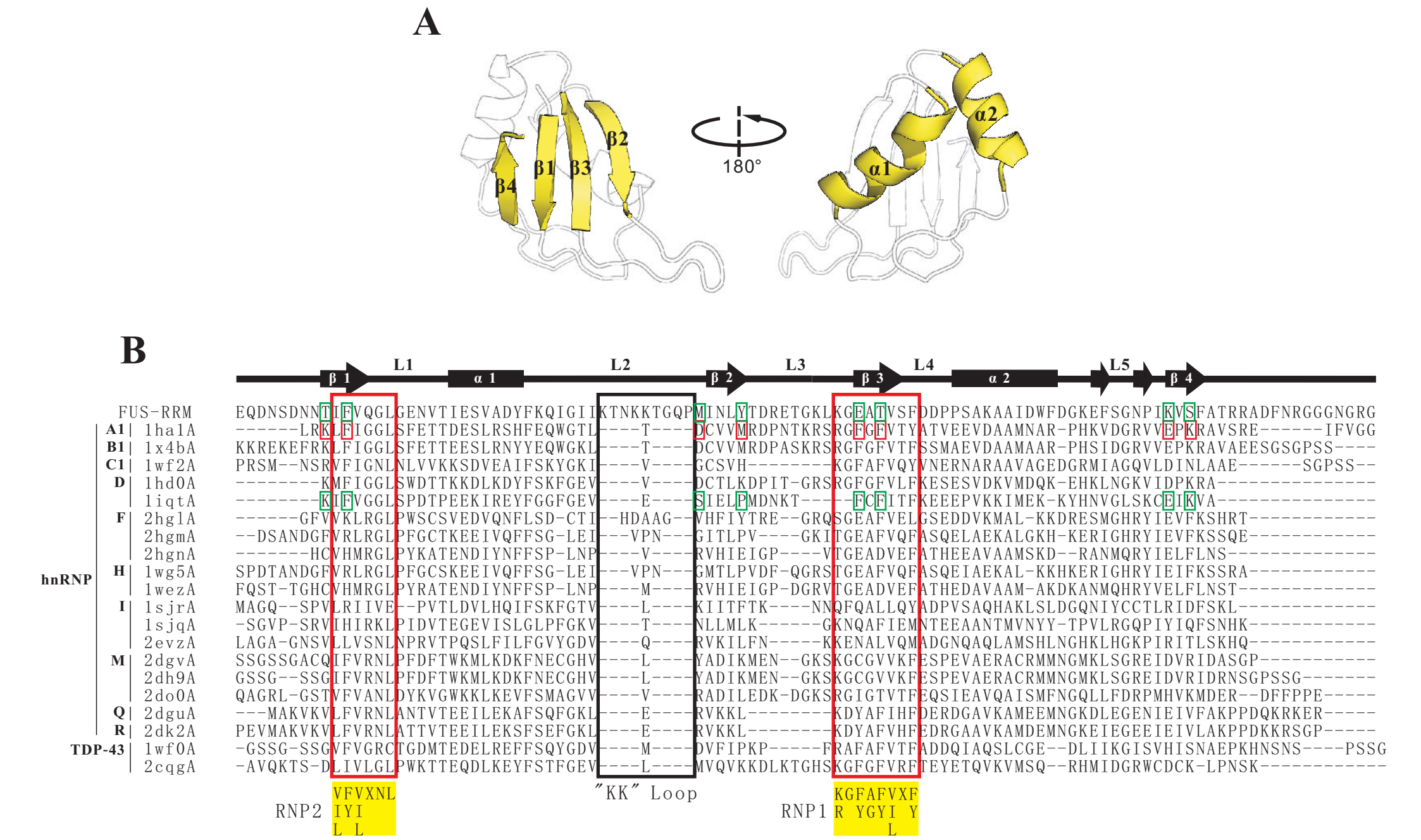
A
β4
β1
β3
β2
180°
α1
α2
B
L1
L2
L3
L4
L5
β 1
α 1
β 2
β 3
α 2
β 4
FUS-RRM
A1| 1ha1A
B1| 1x4bA
C1| 1wf2A
D| 1hd0A
1iqtA
F| 2hg1A
2hgmA
2hgnA
hnRNP
H| 1wg5A
1wezA
I| 1sjrA
1sjqA
2evzA
M| 2dgvA
2dh9A
2do0A
Q| 2dguA
R| 2dk2A
TDP-43| 1wf0A
2cqgA
RNP2
VFVXNL
IYI
L L
"KK" Loop
RNP1
KGFAFVXF
R YGYI Y
L

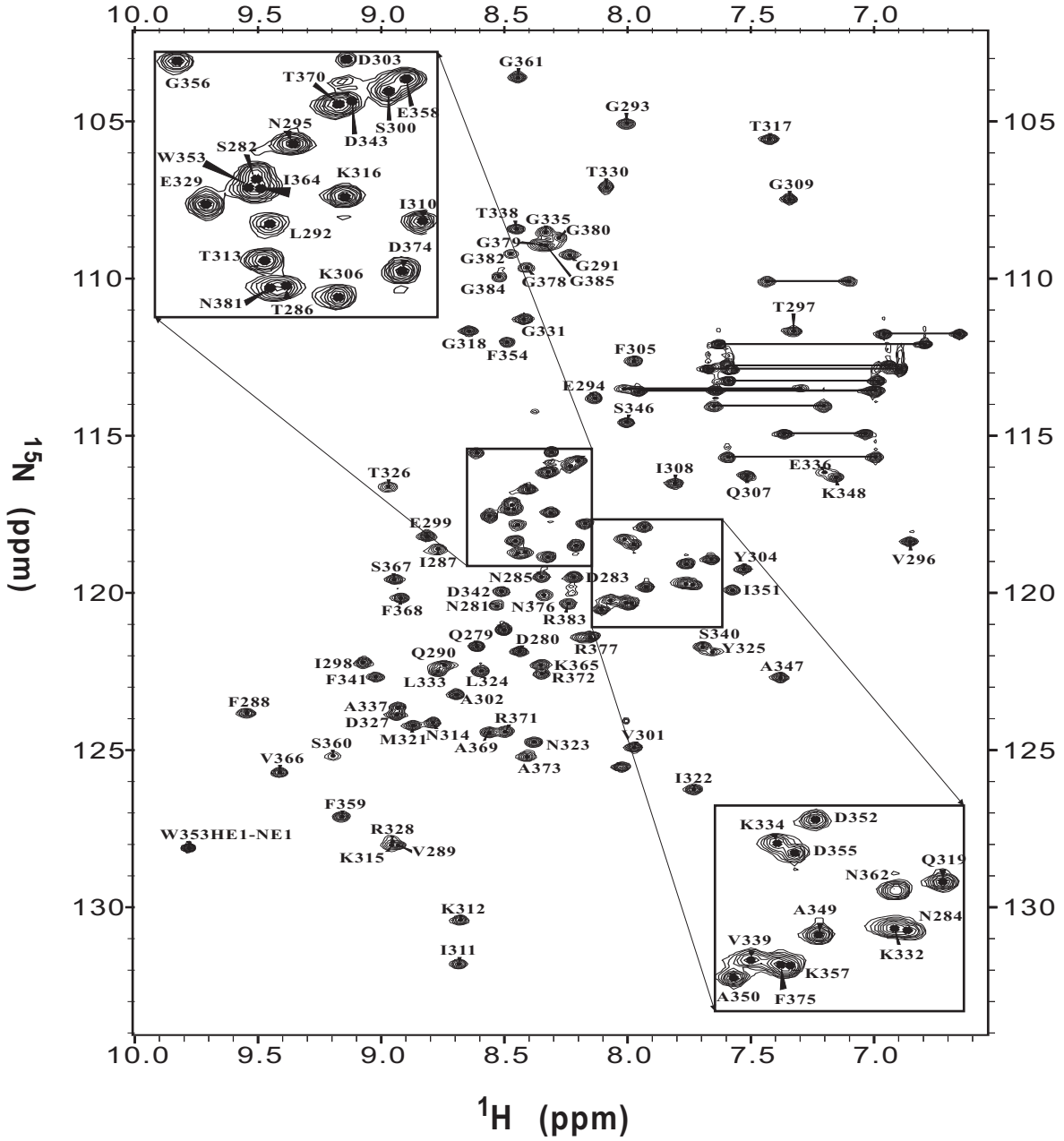
10.0
9.5
9.0
8.5
8.0
7.5
7.0
105
110
115
120
125
130
^{15}N (ppm)
^{1}H (ppm)
G361
G293
T317
T330
G309
T338
G335
G380
G379
G382
G291
G384
G378
G385
T297
G318
G331
F354
F305
E294
S346
T326
I308
E336
Q307
K348
E299
I287
V296
S367
N285
D283
Y304
D342
I351
N281
N376
F368
R383
Q279
D280
S340
R377
Y325
Q290
I298
K365
A347
F341
L333
L324
R372
A302
F288
A337
D327
R371
M321
N314
A369
N323
V301
S360
V366
A373
I322
F359
R328
W353HE1-NE1
K315
V289
K312
I311
K334
D352
D355
Q319
N362
A349
N284
V339
K332
K357
A350
F375
D303
G356
T370
E358
N295
S300
D343
S282
W353
E329
I364
K316
I310
L292
D374
T313
K306
N381
T286

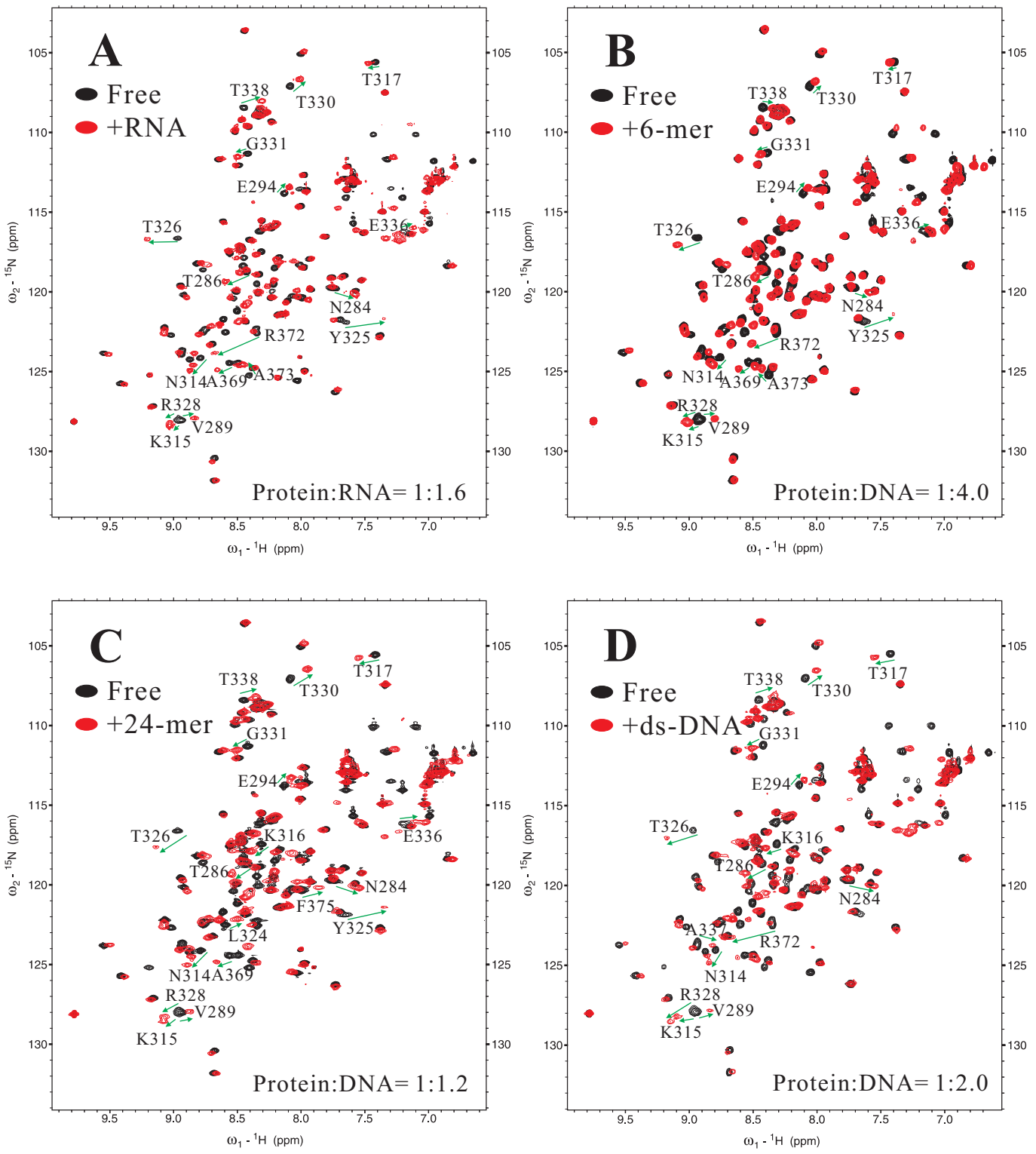
A
Free
+RNA
T338
T330
T317
G331
E294
E336
T326
T286
N284
R372
Y325
N314
A369
A373
R328
V289
K315
Protein:RNA= 1:1.6
B
Free
+6-mer
T338
T330
T317
G331
E294
E336
T326
T286
N284
R372
Y325
N314
A369
A373
R328
V289
K315
Protein:DNA= 1:4.0
C
Free
+24-mer
T338
T330
T317
G331
E294
E336
T326
K316
T286
N284
F375
Y325
L324
N314
A369
R328
V289
K315
Protein:DNA= 1:1.2
D
Free
+ds-DNA
T338
T330
T317
G331
E294
T326
K316
T286
N284
A33
R372
N314
R328
V289
K315
Protein:DNA= 1:2.0
ω2 - 15N (ppm)
ω1 - 1H (ppm)
105
110
115
120
125
130
9.5
9.0
8.5
8.0
7.5
7.0

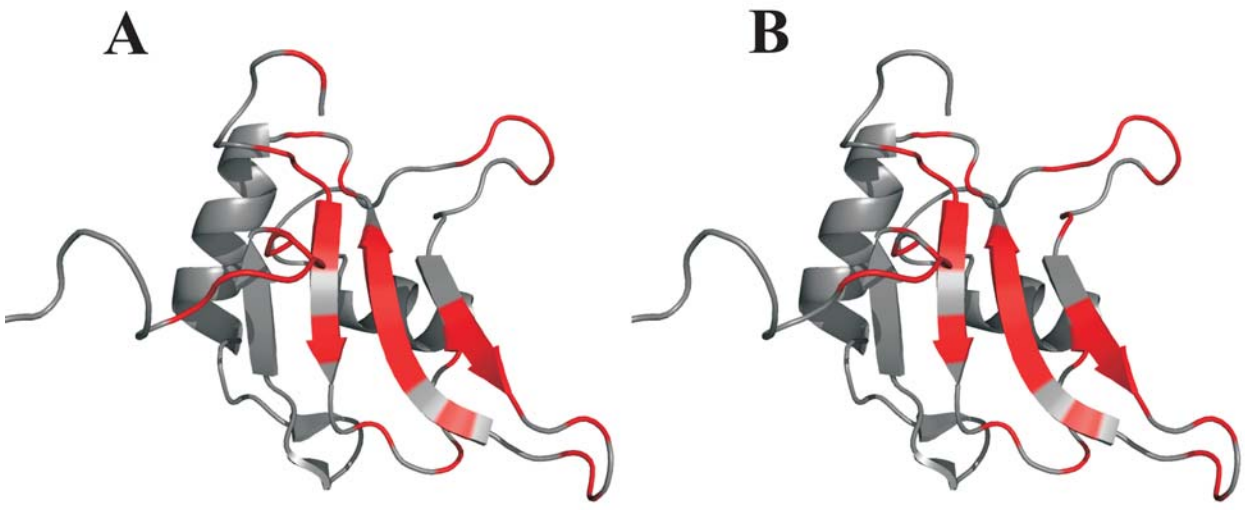

FUS-RRM

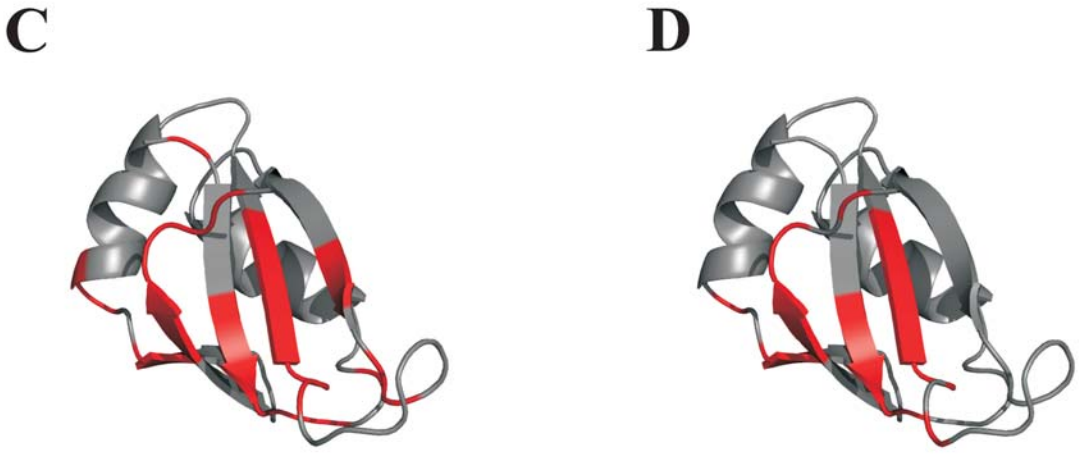

BD2 of hnRNP D

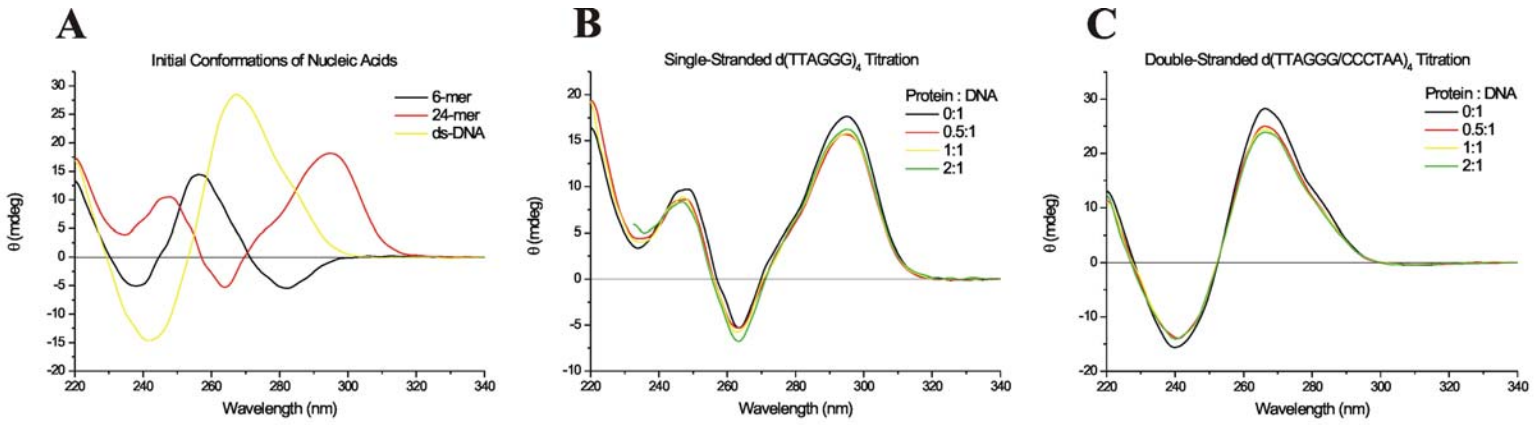
A
Initial Conformations of Nucleic Acids
6-mer
24-mer
ds-DNA
θ (mdeg)
Wavelength (nm)
B
Single-Stranded d(TTAGGG)4 Titration
Protein : DNA
0:1
0.5:1
1:1
2:1
θ (mdeg)
Wavelength (nm)
C
Double-Stranded d(TTAGGG/CCCTAA)4 Titration
Protein : DNA
0:1
0.5:1
1:1
2:1
θ (mdeg)
Wavelength (nm)

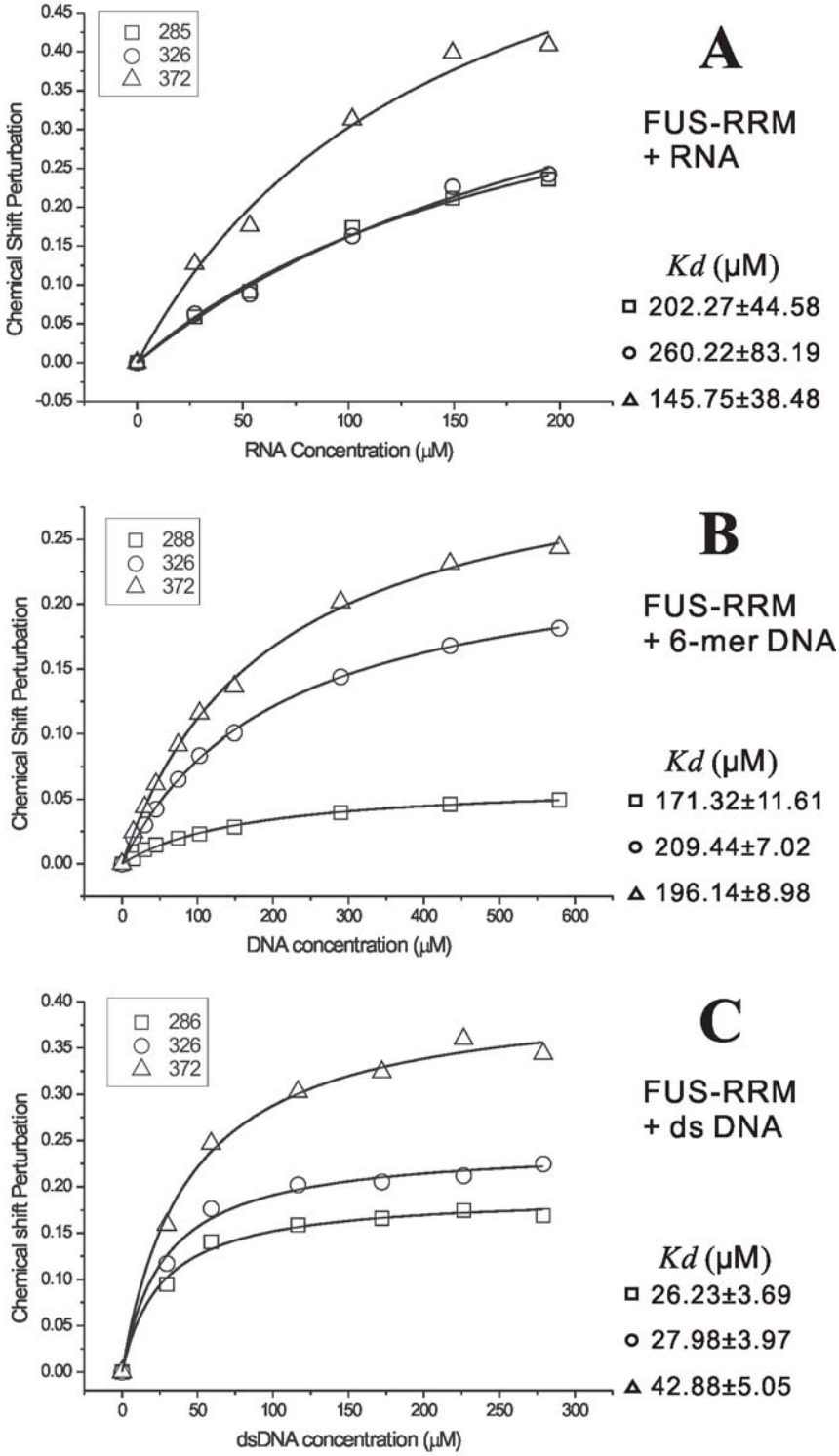
A
FUS-RRM
+ RNA
285
326
372
Chemical Shift Perturbation
RNA Concentration (μM)
Kd (μM)
202.27±44.58
260.22±83.19
145.75±38.48
B
FUS-RRM
+ 6-mer DNA
288
326
372
Chemical Shift Perturbation
DNA concentration (μM)
Kd (μM)
171.32±11.61
209.44±7.02
196.14±8.98
C
FUS-RRM
+ ds DNA
286
326
372
Chemical shift Perturbation
dsDNA concentration (μM)
Kd (μM)
26.23±3.69
27.98±3.97
42.88±5.05

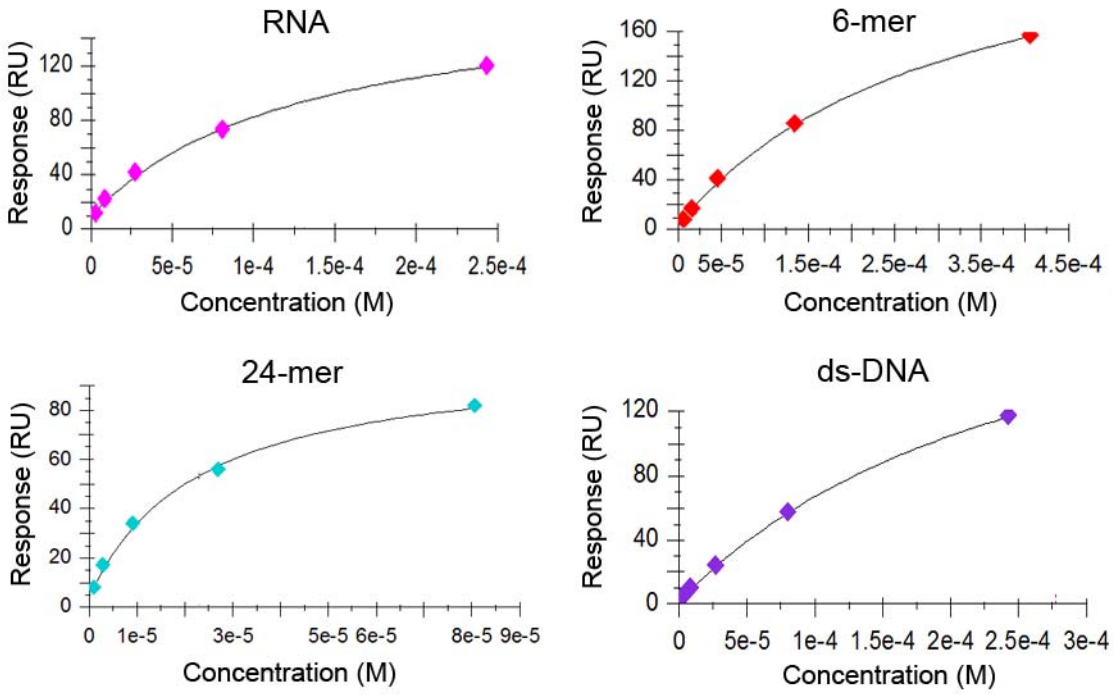
RNA
Response (RU)
120
80
40
0
0
5e-5
1e-4
1.5e-4
2e-4
2.5e-4
Concentration (M)
6-mer
Response (RU)
160
120
80
40
0
0
5e-5
1.5e-4
2.5e-4
3.5e-4
4.5e-4
Concentration (M)
24-mer
Response (RU)
80
60
40
20
0
0
1e-5
3e-5
5e-5
6e-5
8e-5
9e-5
Concentration (M)
ds-DNA
Response (RU)
120
80
40
0
0
5e-5
1e-4
1.5e-4
2e-4
2.5e-4
3e-4
Concentration (M)

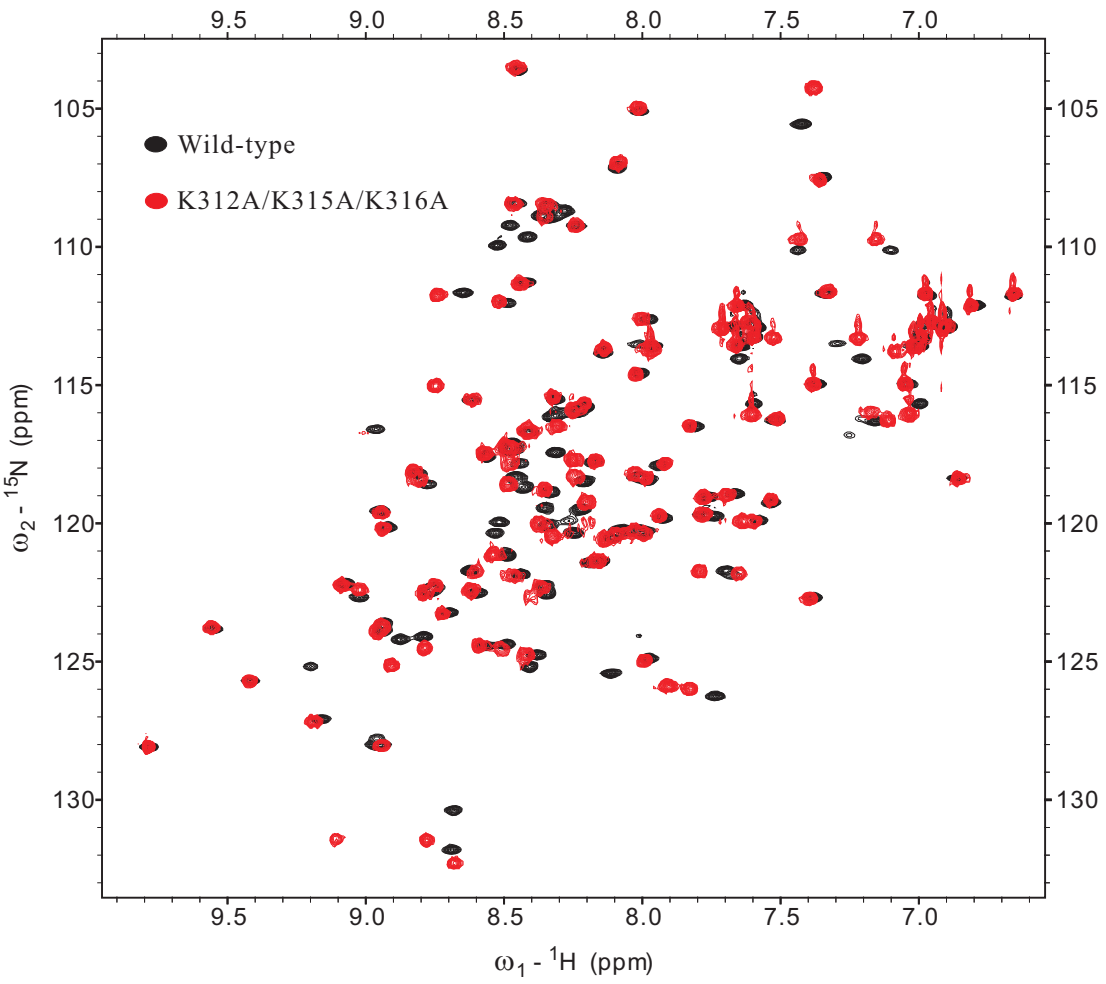
Wild-type
K312A/K315A/K316A
9.5
9.0
8.5
8.0
7.5
7.0
105
110
115
120
125
130
ω2 - 15N (ppm)
ω1 - 1H (ppm)